



## A Finite volume simulation of a supersonic laminar Flow: Application to a compression corner

D. Bahia<sup>1,2</sup>, N. Salhi<sup>3</sup>

1. Department of Physics, Multidisciplinary Faculty of Nador, University of Mohammed Premier Oujda, Morocco
2. Laboratory: Observatoire de la Lagune Marchica de Nador et Régions Limitrophes (OLMAN-RL)
3. Department of Physics, Faculty of Sciences of Oujda, University of Mohammed Premier Oujda, Morocco

Received 16 Jan 2017,  
Revised 23 May 2017,  
Accepted 24 May 2017

### Keywords

- ✓ Navier-Stokes;
- ✓ Numerical analysis;
- ✓ Supersonic flow;
- ✓ Finite volume;
- ✓ Compression corner

D BAHIA  
[drisbahia1971@yahoo.fr](mailto:drisbahia1971@yahoo.fr)  
+212648364584

### Abstract

In this paper, the finite volume method is used for the computation of a supersonic laminar flow. As an application, we consider the flow over a compression corner with different angles. The inviscid fluxes are approximated using Steger and Warming Flux Vector Splitting method with the MUSCL approach to increase the spatial accuracy. The transport properties (viscosity and conductivity) which are functions of two independent thermodynamic parameters (T, P), are calculated using a centered scheme. The performance of the method that is used here is shown by some comparisons with other results.

## 1. Introduction

Viscous interaction is one of the major aspects of supersonic flows. The interaction between a shock wave and a boundary layer can produce a region of separated flow [1].

Mac Cormack method was one of the most popular of the central schemes [2]. Space-centered schemes of second order accuracy in space were initially introduced with implicit linear multi-step time integration methods by Briley and McDonald [3], and Beam and Warming [4]. Due to the oscillations that are created in central algorithm, Up wind schemes were introduced to prevent these oscillations.

The first explicit Up wind scheme was introduced by Courant, Isaacson and Reeves (1952), since this date there has been considerable effort aimed at constructing and analyzing high order accurate, non-oscillatory approximations to hyperbolic conservation laws [5-6]. First Van Leer published his work on the "Ultimate difference schemes" in a series of traditional papers [7-11]. This work represented a complete extension of the idea of Godunov to high order schemes. Currently, one of the most popular solvers is due to Roe [12], who proposed a linearized Riemann solver for the Euler equations, where the thermodynamic properties are represented by the perfect gas law. Since 1981, several generalizations of the Roe solver were proposed in order to include the effects real gases [13-15]. More recently, Gallout and Masella [16], presented a numerical scheme, VFRoe, of finite volume type for the system of nonlinear one-dimensional hyperbolic equations.

Flat plate and compression corner flows appear in many supersonic aircraft configurations and particularly interesting feature is the interaction of a boundary layer with shock waves. Within this framework several works were completed knowing that the work of Carter J. [17] is the reference of all work since 1972. Rizzetta D. [18]; Tenaud C. [19]; Mallinson S. G. [20]; Fang J. [21]; Jammalamadaka et al. [22]; Yang G., Yao Y., Fang J., Gan T. [23] are considered as members of the same subgroup who treat the compressible supersonic flows on a compression corner with different methods.

In this work, a second order finite volume method is used for the resolution of a supersonic laminar flow over a compression corner, on a general quadrilateral meshes. The paper is organized as follows: the governing equations are given in section 2; section 3 describes the finite volume approach and the numerical flux approximation. The numerical tests and comparisons with others results are showed in section 4.

## 2. Presentation

The compressible viscous flow is described by the conservation laws of total mass, momentum and energy. This system of conservation equations can be written in a general integral form, which is the basis of the finite volume method, described later [1]. For an arbitrary control volume  $\Omega$ , surrounded by the surface  $S$ , the equations write

$$\frac{\partial}{\partial t} \int_{\Omega} U \, d\Omega + \left[ \int_S \vec{F}_c \cdot d\vec{S} + \int_S \vec{F}_d \cdot d\vec{S} \right] = 0 \quad (1)$$

Where  $U$  is the vector of conservative variables,  $\vec{F}_c$  and  $\vec{F}_d$  are the flux vectors of the inviscid and viscous contributions, respectively.

$$U = \begin{pmatrix} \rho \\ \rho \vec{V} \\ \rho E \end{pmatrix} \quad \vec{F}_c = \begin{pmatrix} \rho \vec{V} \\ \rho \vec{V} \otimes \vec{V} + P \bar{I} \\ \rho H \vec{V} \end{pmatrix} \quad \vec{F}_d = \begin{pmatrix} 0 \\ \bar{\tau} \\ \bar{\tau} \cdot \vec{V} - k \vec{\nabla} T \end{pmatrix}$$

$\vec{V}$  is the velocity vector,  $\rho$  is the mass density,  $P$  the pressure,  $T$  the temperature,  $E$  the total energy per mass and  $k$  is the thermal conductivity. The components of the shear stress are given by

$$\bar{\tau}_{ij} = \mu \left( \frac{\partial v_i}{\partial x_j} + \frac{\partial v_j}{\partial x_i} \right) - \frac{2}{3} \mu (\vec{\nabla} \cdot \vec{V}) \delta_{ij}$$

$\mu$  is the dynamic viscosity of the flow,

$\delta_{ij}$  is the symbol of Kronecker.

To close this system, the equation of state for the pressure has to be added:

$$P = \frac{\gamma - 1}{\gamma} \rho T \quad (2)$$

$\gamma$  is the ratio of specific heats.

The variables in equations (1) and (2) may be nondimensionalized as follows:

$$\begin{aligned} x^* &= \frac{x}{L} & y^* &= \frac{y}{L} \\ u^* &= \frac{u}{U_{\infty}} & v^* &= \frac{v}{U_{\infty}} & t^* &= \frac{tL}{U_{\infty}} \\ \rho^* &= \frac{\rho}{\rho_{\infty}} & P^* &= \frac{P}{\rho_{\infty} U_{\infty}^2} & T^* &= \frac{c_p T}{U_{\infty}^2} \\ E^* &= \frac{E}{\rho_{\infty} U_{\infty}^2} & \mu^* &= \frac{\mu}{\mu_{\infty}} \end{aligned}$$

Where:

$c_p$  is the specific heat at constant pressure,  $L$  is the length of the plate.  $U_{\infty}$  is the reference velocity,  $\rho_{\infty}$  is the reference density,  $\mu_{\infty}$  is the reference viscosity and  $\infty$  is the free stream symbol.

The resulting system of nondimensionalized differential equations may be conveniently as:

$$\frac{\partial}{\partial t^*} \int_{\Omega} U^* \, d\Omega + \left[ \int_S \vec{F}_c^* \cdot d\vec{S} + \int_S \vec{F}_d^* \cdot d\vec{S} \right] = 0 \quad (3)$$

$$U^* = \begin{pmatrix} \rho^* \\ \rho^* \vec{V}^* \\ \rho^* E^* \end{pmatrix} \quad \vec{F}_c^* = \begin{pmatrix} \rho^* \vec{V}^* \\ \rho^* \vec{V}^* \otimes \vec{V}^* + P^* \bar{I} \\ \rho^* H^* \vec{V}^* \end{pmatrix} \quad \vec{F}_d^* = \frac{1}{\text{Re}_{\infty, L}} \begin{pmatrix} 0 \\ \bar{\tau}^* \\ \bar{\tau}^* \cdot \vec{V}^* - \frac{\mu^*}{\text{Pr}} \vec{\nabla} T^* \end{pmatrix}$$

With:

$Re_{\infty,L}$  is the Reynolds number,  $Re_{\infty,L} = \frac{\rho_{\infty} U_{\infty} L}{\mu_{\infty}}$ , Pr is the Prandtl number.

And:

$$\tau_{ij}^* = \mu^* \left( \frac{\partial v_i^*}{\partial x_j^*} + \frac{\partial v_j^*}{\partial x_i^*} \right) - \frac{2}{3} \mu^* (\nabla \cdot \vec{V}^*) \delta_{ij} \quad P^* = \frac{\gamma - 1}{c_p \gamma} \rho^* T^*$$

### 3. Finite volume discretization

The basic idea of a finite volume method is to use a finite set of control volumes to describe the equation and restrict the unknown to be in a finite dimensional space [24].

Within this approach the integral conservation laws are written for a discrete 2D control volume (ABCD), called cell (i, j) (figure 1).

Equation (3) is replaced by the discretized form:

$$\frac{\partial}{\partial t^*} (U_{ABCD}^* \cdot \Omega_{ABCD}) + \sum_{sides} (\vec{F}_c^* + \vec{F}_d^*) \cdot \vec{S} = 0 \quad (4)$$

Where the sum of the flux terms refers to all the external sides of the control cell (ABCD). We would identify  $U_{ABCD}^*$  with  $U_{ij}^*$ ,  $\Omega_{ABCD}$  with the area of (ABCD).

$$\frac{\partial U_{ij}^*}{\partial t^*} = - \frac{1}{\Omega_{ABCD}} \sum_{4 \text{ faces}} (\vec{F}_c^* + \vec{F}_d^*) \cdot \vec{S} = 0 \quad (5)$$

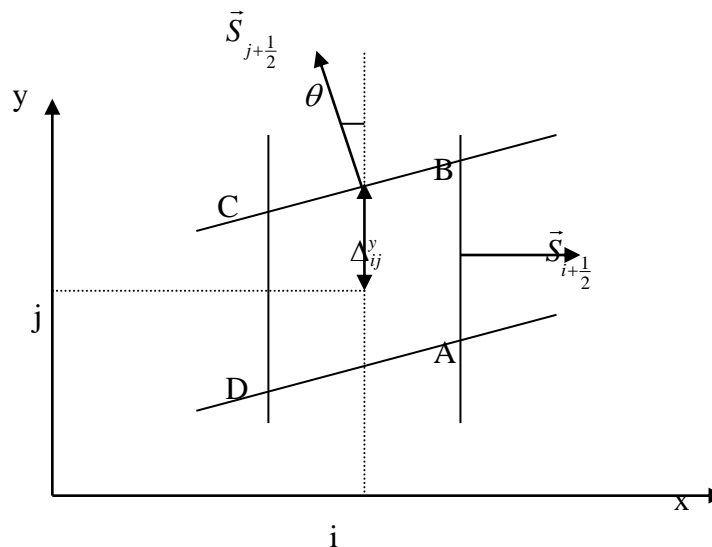


**Figure 1:** Two dimensional control volumes

The evaluation of the term  $\frac{\partial U_{ij}^*}{\partial t^*}$  in equation (5) determines whether the scheme is explicit or implicit and fixes the time accuracy.

#### 3.1 Convective flux

There are several ways to carry out the convection flux [25-26]. Here we present an upwind scheme based on the "Flux Vector Splitting" method of Steger and Warming [27]. The idea is to seek the characteristic lines of the flow on which the physical information is propagated and to discretize the flux according to this direction. The flux is decomposed into a positive part and a negative part according to the direction of the transport on these characteristic lines.

The positive fluxes are evaluated using available information in the cells upstream of the normal  $\vec{S} = S \cdot \vec{n}$ , and vice versa for the negative fluxes.

This splitting of the convective flux is based on the sign of the eigenvalues of the jacobian  $\vec{A} \cdot \vec{n}$  we write:

$$\left[ \vec{F}_c \cdot \vec{n} \right]_{side} = \left[ \left( \vec{A} \cdot \vec{n} \right) U^* \right]_{side} = \left[ \left( P(\vec{n}) \cdot D(\vec{n}) \cdot P^{-1}(\vec{n}) \right) U^* \right]_{side} \quad (6)$$

Where  $P(\vec{n})$  and  $D(\vec{n})$  are respectively, the transformation matrix and the diagonal matrix. The eigenvalues of the Jacobian matrix of the system are:

$$\lambda_1 = \lambda_2 = \vec{V}^* \cdot \vec{n}; \quad \lambda_3 = \vec{V}^* \cdot \vec{n} + c; \quad \lambda_4 = \vec{V}^* \cdot \vec{n} - c$$

Where  $c$  is the speed of the sound:  $c^2 = \frac{\gamma P^*}{\rho^*}$

We decompose the diagonal matrix  $D$  as:  $D = D^+ + D^-$

The matrix  $D^+$  contains only the positive terms  $\lambda_j^+$  and vice versa for the matrix  $D^-$  :

$$\lambda_j^{+-} = \frac{1}{2} (\lambda_j \pm |\lambda_j|)$$

$$\alpha = 2(\gamma - 1)\lambda_1^{+-} + \lambda_3^{+-} + \lambda_4^{+-}$$

What gives:

$$\left[ \vec{F}_c \cdot \vec{n} \right]_{side} = \left[ \left( P(\vec{n}) \cdot D(\vec{n}) \cdot P^{-1}(\vec{n}) \right) U^* \right]_{side} = \left[ \left( P(\vec{n}) \cdot D^+(\vec{n}) \cdot P^{-1}(\vec{n}) \right) U^* \right]_{side} + \left[ \left( P(\vec{n}) \cdot D^-(\vec{n}) \cdot P^{-1}(\vec{n}) \right) U^* \right]_{side} = \left[ \vec{F}_c \cdot \vec{n} \right]_{side}^+ + \left[ \vec{F}_c \cdot \vec{n} \right]_{side}^- \quad (7)$$

In the 2D the following expressions are obtained from the split convective fluxes:

$$\left[ \vec{F}_c \cdot \vec{n} \right]_{side}^{+-} = \frac{\rho^*}{2\gamma} \begin{cases} \alpha \\ \mathbf{u}^* \alpha + c n_x (\lambda_3^{+-} - \lambda_4^{+-}) \\ \mathbf{v}^* \alpha + c n_y (\lambda_3^{+-} - \lambda_4^{+-}) \\ \alpha \frac{\mathbf{u}^{*2} + \mathbf{v}^{*2}}{2} + \frac{c^2}{\gamma - 1} (\lambda_3^{+-} + \lambda_4^{+-}) + c (\vec{V}^* \cdot \vec{n}) (\lambda_3^{+-} - \lambda_4^{+-}) \end{cases} \quad (8)$$

where:

$$\alpha = 2(\gamma - 1)\lambda_1^{+-} + \lambda_3^{+-} + \lambda_4^{+-}$$

$\vec{n} = (n_x, n_y)$  is the outward unit normal vector of the calculation face.

### The spatial accuracy

The simplest upwind scheme results if a zero-order extrapolation of the conservative variables is used:

$$\left[ \vec{F}_c \cdot \vec{n} \right]_{i+\frac{1}{2},j}^+ = \left[ \vec{F}_c \cdot \vec{n} \right]_{i,j}^+$$

$$\left[ \vec{F}_c \cdot \vec{n} \right]_{i+\frac{1}{2},j}^- = \left[ \vec{F}_c \cdot \vec{n} \right]_{i+1,j}^-$$

The resulting scheme is only first-order accurate in space.

Higher order schemes can be obtained using a linear extrapolation of the conservative variables.

This linear extrapolation is performed by using a quasi-1D approach.

For example, the conservative variables on the boundary surface  $(i+1/2, j)$  will be obtained by extrapolating the conservative variables in the nodes  $(i-1, j)$ ,  $(i, j)$ ,  $(i+1, j)$  and  $(i+2, j)$ .

The conservative variables used in the positive split fluxes are denoted  $U_{i+\frac{1}{2},j}^{*+}$  whereas  $U_{i+\frac{1}{2},j}^{*-}$  stands for the values used in the negative split fluxes.

The following extrapolation formulas are used:

$$\begin{cases} U_{AB}^{*+} = U_{ij}^* + \psi(R_{ij}^x) \left[ U_{ij}^* - U_{i-1,j}^* \right] \frac{\Delta_{ij}^x}{\Delta_{i-1,j}^x + \Delta_{ij}^x} \\ U_{AB}^{*-} = U_{i+1,j}^* + \psi\left(\frac{1}{R_{i+1,j}^x}\right) \left[ U_{i+1,j}^* - U_{i+2,j}^* \right] \frac{\Delta_{ij}^x}{\Delta_{i+1,j}^x + \Delta_{i+2,j}^x} \end{cases} \quad (9)$$

Where the function  $\psi$  is defined as:

$$\psi(R_{ij}^x) = \frac{1-k}{2} + \frac{1+k}{2} R_{ij}^x$$

$R_{ij}^x$  is the ratio of the gradients downstream and upstream of the cell (i, j) :

$$R_{ij}^x = \frac{U_{i+1,j}^* - U_{i,j}^*}{U_{i,j}^* - U_{i-1,j}^*} \frac{\Delta_{i,j}^x - \Delta_{i-1,j}^x}{\Delta_{i,j}^x - \Delta_{i+2,j}^x}$$

with:

$$\Delta_{ij}^x = \left[ \left( x_{i+\frac{1}{2},j}^* - x_{i,j}^* \right)^2 + \left( y_{i+\frac{1}{2},j}^* - y_{i,j}^* \right)^2 \right]^{\frac{1}{2}}$$

The extrapolation ensures that the scheme is of second-order accuracy in space.

The parameter defines different schemes. The most values currently used are  $k=-1$  (fully upwind scheme),  $k=0$  (partially upwind scheme).

It is clear that the higher order schemes are not monotonous. This may lead to oscillations into the solution especially in the vicinity of large gradients such as shocks. In order to restore monotonicity limiters which are introduced in the extrapolation formulas.

This leads to a redefinition of the function  $\psi$  :

$$\psi(R_{ij}^x) = \left[ \frac{1-k}{2} + \frac{1+k}{2} R_{ij}^x \right] \times \text{Lim}$$

The following limiter of Minmod is used:

$$\text{Lim} = \begin{cases} 0 & \text{if } R_{ij} \leq 0 \\ R_{ij} & \text{if } 0 < R_{ij} < 1 \\ 1 & \text{if } R_{ij} \geq 1 \end{cases} \quad (10)$$

### 3.2 Diffusive flux

Because of the elliptic character of the diffusive flux [1] (the physical information is propagated everywhere), the viscous and thermal diffusion terms are computed here by a second-order centered scheme. First, the flux is decomposed in the two directions as follow

$$\sum_{4 \text{ faces}} (\vec{F}_d) = \sum_{4 \text{ faces}} (F_d^{*x} \cdot \mathbf{n}_x) + \sum_{4 \text{ faces}} (F_d^{*y} \cdot \mathbf{n}_y) \quad (11)$$

with :

$$F_d^{*x} = - \begin{bmatrix} 0 \\ \frac{2}{3} \mu^* \left( 2 \frac{\partial u^*}{\partial x^*} - \frac{\partial v^*}{\partial y^*} \right) \\ \mu^* \left( \frac{\partial u^*}{\partial y^*} - \frac{\partial v^*}{\partial x^*} \right) \\ \frac{4\mu^*}{3} u^* \frac{\partial u^*}{\partial x^*} - \frac{2\mu^*}{3} u^* \frac{\partial v^*}{\partial y^*} + \mu^* v^* \frac{\partial u^*}{\partial y^*} + \mu^* v^* \frac{\partial v^*}{\partial x^*} + k^* \frac{\partial T^*}{\partial x^*} \end{bmatrix} \quad F_d^{*y} = - \begin{bmatrix} 0 \\ \mu^* \left( \frac{\partial u^*}{\partial y^*} + \frac{\partial v^*}{\partial x^*} \right) \\ \frac{2}{3} \mu^* \left( 2 \frac{\partial v^*}{\partial y^*} - \frac{\partial u^*}{\partial x^*} \right) \\ \frac{4\mu^*}{3} u^* \frac{\partial v^*}{\partial y^*} - \frac{2\mu^*}{3} v^* \frac{\partial u^*}{\partial x^*} + \mu^* u^* \frac{\partial u^*}{\partial y^*} + \mu^* u^* \frac{\partial v^*}{\partial x^*} + k^* \frac{\partial T^*}{\partial y^*} \end{bmatrix}$$

The derivatives acquiring in the expressions for  $F_d^{*x}$  and  $F_d^{*y}$  are found by averaging the mean derivatives in the corner nodes of the cells.

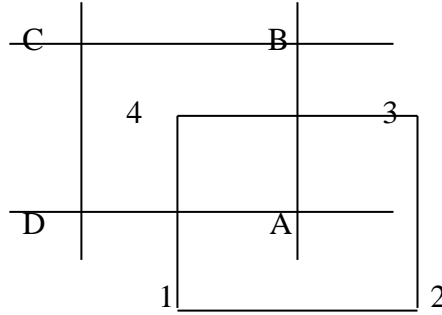


**Figure 2:** The mesh for the discretization of the diffusion flux

We calculate the gradient on the face AB of Figure 2 with:

$$\left. \frac{\partial u^*}{\partial x^*} \right)_{AB} = \frac{1}{2} \left[ \left. \frac{\partial u^*}{\partial x^*} \right)_A + \left. \frac{\partial u^*}{\partial x^*} \right)_B \right] \quad (12)$$

Then we compute the gradient at point A as the mean value of the one on the surrounded cell (1234):

$$\begin{aligned} \left. \frac{\partial u^*}{\partial x^*} \right)_{AB} &= \frac{1}{\Omega_{1234}} \int_{\Omega_{ABCD}} \frac{\partial u^*}{\partial x^*} d\Omega = \frac{1}{\Omega_{1234}} \iint_{S_{1234}} u^* dy^* \\ &= \frac{(u_2^* - u_4^*)(y_3^* - y_1^*) - (u_3^* - u_1^*)(y_2^* - y_4^*)}{(x_2^* - x_4^*)(y_3^* - y_1^*) - (x_3^* - x_1^*)(y_2^* - y_4^*)} \end{aligned} \quad (13)$$

A similar relation is found for the derivative with respect to y:

$$\begin{aligned} \left. \frac{\partial u^*}{\partial y^*} \right)_{AB} &= \frac{1}{\Omega_{1234}} \int_{\Omega_{ABCD}} \frac{\partial u^*}{\partial y^*} d\Omega = \frac{1}{\Omega_{1234}} \iint_{S_{1234}} u^* dx^* \\ &= \frac{(x_2^* - x_4^*)(u_3^* - u_1^*) - (x_3^* - x_1^*)(u_2^* - u_4^*)}{(x_2^* - x_4^*)(y_3^* - y_1^*) - (x_3^* - x_1^*)(y_2^* - y_4^*)} \end{aligned} \quad (14)$$

### 3.3 Time integration

We use a first-order explicit scheme for the discretization in time; therefore the Eq. (3) becomes:

$$U_{ij}^{n+1*} = U_{ij}^{n*} - \frac{\Delta t^*}{\Omega_{ABCD}} \left[ \sum_{4sides} (\vec{F}_c^* \cdot \vec{S}) + \sum_{4sides} (\vec{F}_d^* \cdot \vec{S}) \right] \quad (15)$$

### Stability analysis

The scheme (15) described above is applied to the 2D linear convection-diffusion equation:

$$\frac{\partial u^*}{\partial t^*} + a \left( \frac{\partial u^*}{\partial x^*} + \frac{\partial u^*}{\partial y^*} \right) = \nu \left( \frac{\partial^2 u^*}{\partial x^{*2}} + \frac{\partial^2 u^*}{\partial y^{*2}} \right) \quad (16)$$

$\nu$  is the kinematic viscosity of the flow.

Neumann analysis on the stability of the scheme described before give the following stability condition:

$$\Delta t^* \leq \frac{0.5 \text{ Pr Re}_{\infty, L}}{\gamma \left( \frac{\mu}{\rho} \right) \left( \frac{1}{\Delta x^{*2}} + \frac{1}{\Delta y^{*2}} \right)} \quad (17)$$

where  $\Delta t^*$  is time step, and  $\Delta x^*$  and  $\Delta y^*$  are the spatial steps.

## 4. Results and discussion: Supersonic flow over a compression corner with angles of 5, 7.5 and 10

In this Navier-Stokes problem, a Mach 3 flow passes over a compression corner at an angle of 5°, 7.5° and 10°. The Reynolds number, based on the free-stream values and the distance from the leading edge of the flat to the

corner, is 16800. The geometry of the physical domain and the way of grid used are shown in the figure 3 below.

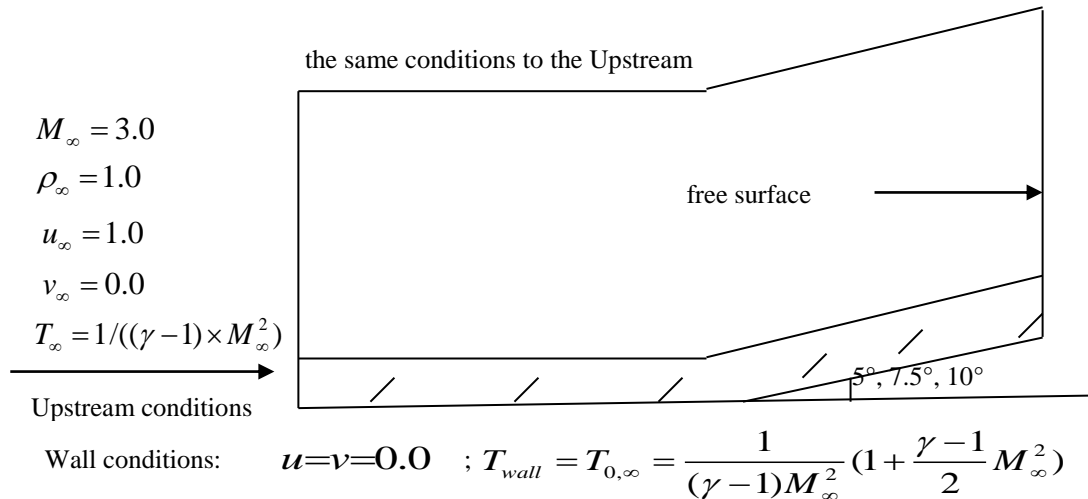


**Figure 3:** The Mach 3 flow over compression corner with angles of 5°, 7.5° and 10°

The computational domain covers the area  $0 \leq x^* \leq 2.0$ ,  $0 \leq y^* \leq 0.575$  on the plate, and a height of 0.575 above the wall past the corner. The leading-edge of the plate is placed at  $x^* = 0$  and the corner at  $x^* = 1$ . The total number of grid points used was 2156, thereby a constant grid spacing in the  $x^*$  and  $y^*$  directions.

Figure 4 shows the wall pressure distribution for ramp angles of 5, 7.5 and 10. It is seen that the pressure is a decreasing function on  $0 \leq \frac{x}{x_c} \leq 0.7$  and it is an increasing function on  $0.7 \leq \frac{x}{x_c} \leq 2$ . The profiles possess discontinuities at the corner  $\frac{x}{x_c} = 1$ .

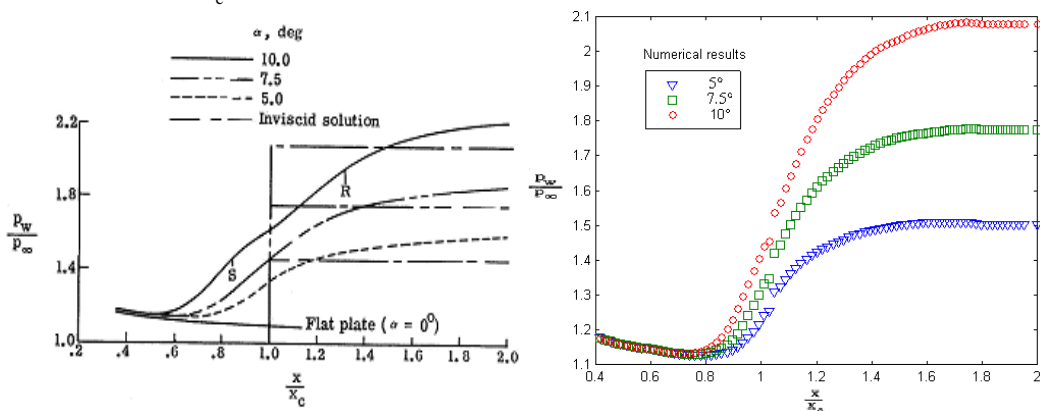


**Figure 4:** Comparison of wall pressure distribution for Ramp angles of 5°, 7.5° and 10°

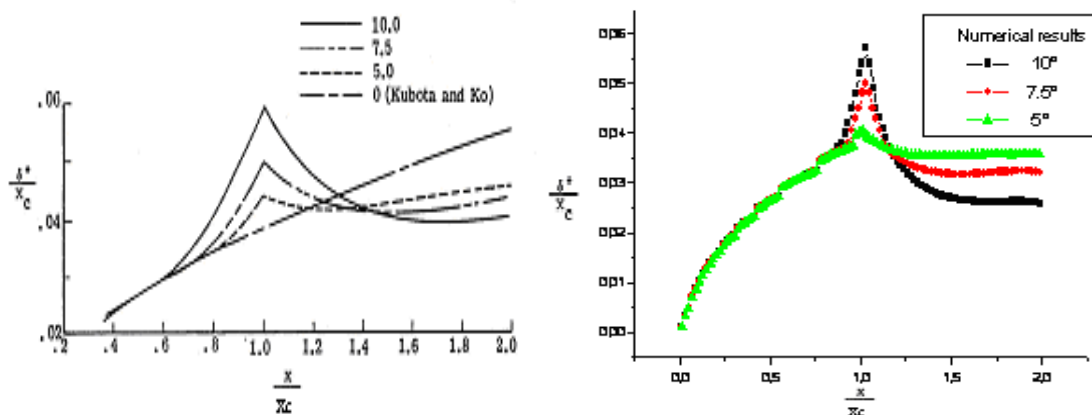


**Figure 5:** Comparison of the displacement thickness measured normal to the surface distribution for different ramp angles

Figure 5 presents the displacement thickness distribution. The profiles are composed of two parts, the first part is an increasing function and the second one is a decreasing function. The profiles possess a maximum at the corner. This maximum value is more important for ramp angle  $10^\circ$ .

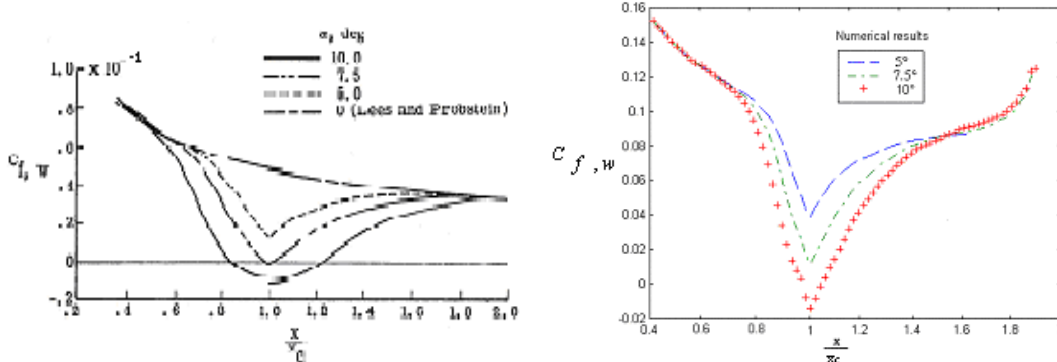


**Figure 6:** Comparison of wall skin-friction distribution for different ramp angles

Figure 6 presents the skin-friction distribution. Here also, the profiles are composed of two parts, the first part is a decreasing function and the second is an increasing function. The profiles possess a minimum at the corner. This minimum value is more important for the ramp angle  $10^\circ$ .

These results show good agreement with the results of Carter J. [17], Fang J. [21] and Babinsky H. [31].

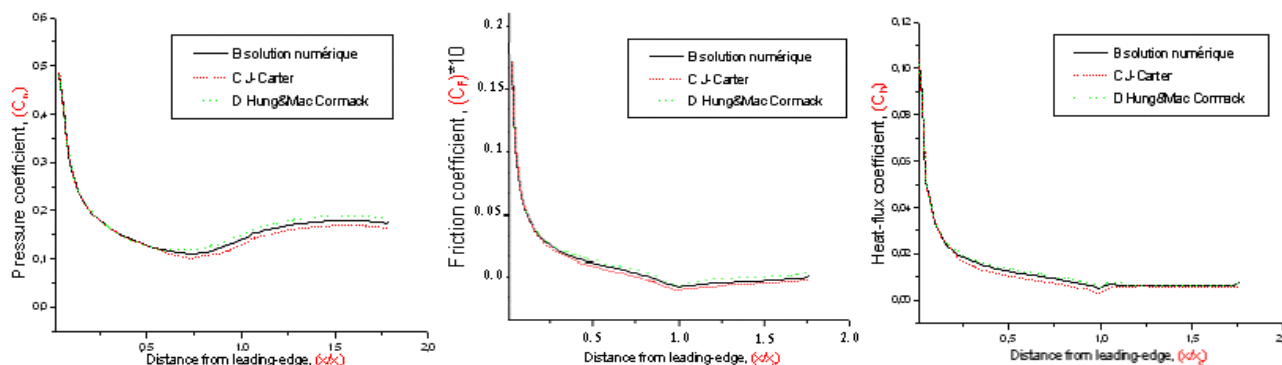


**Figure 7:** Comparison of the results of present calculation and the results of Carter J. and Hung & Mac Cormack

Figure 7 presents the profiles of the friction coefficient, heat-flux coefficient and pressure coefficient along the wall, the results of present calculation show good agreement with the results of Carter J. [17], Hung C. M., Mc Cormack R. W. [26] and Jammalamadaka A. [22].

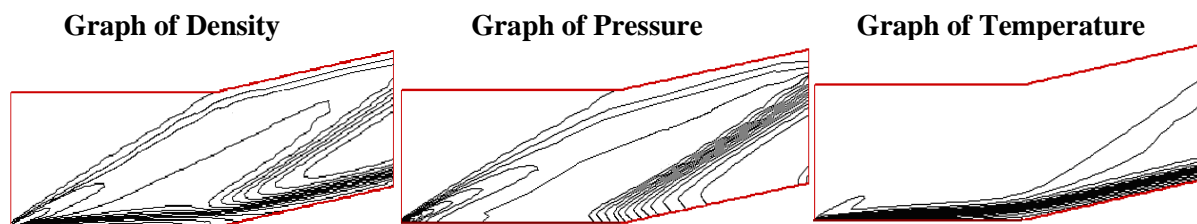


**Figure 8:** Solution of the Mach 3 compression corner problem

Figure 8 shows the profiles of adiabatic and isotherm contours, this figure demonstrates the ability of the method to capture the leading-edge shock, the results of present calculation show good agreement with the results of Carter J. [17], Yang G. [23], WU M. & Martin M. P. [28], Babinsky H. & Harvey J. K. [29] and Zapryagaev V. I., Kavun I. N. & Lipatov I. I. [30].

The number of cycle required for convergence of the calculations discussed was 500. However for the calculation carried out by J. Carter there is 1500 to 3000.

## Conclusions

This paper presents a numerical simulation of the Navier -Stokes equations that govern a supersonic laminar flow over a compression corner.

An upwind second order finite volume scheme is used for the discretization of the convective fluxes, on general quadrilateral meshes, whereas the diffusive contributions are computed with a centered scheme.

The results of the test case considered here and the comparisons made with the results of Fang J. [21], Jammalamadaka A. [22], Yang G. [23], WU M. [28], Babinsky H. [29] and Zapryagaev V. I. [30] show the good performance of the algorithms employed.

## References

1. Hirsch C., *Vol. 2.* (1990).
2. Mc Cormack R. W., *J. AIAA. 4th Aerodynamic Testing Conference.* 4 (1969) 354.
3. Briley W. R., Mc Donald H., *Proc. of the 4<sup>th</sup> Int. Conf. on Numerical Methods in Fluid Dynamics.* 35 (1975) 273.
4. Beam R. M., Warming R. F., *J. Comp. Physics.* 22 (1976) 87.
5. Harten A., *J. Publ Res I Math Sci.* 7 (1987) 147.
6. Boris J. P., *J. Comp. Physics.* 11 (1973) 38.
7. Van Leer B., *Springer Lecture Notes in Physics.* 18 (1973) 163.
8. Van Leer B., *J. Comp. Physics.* 18 (1974) 361.
9. Van Leer B., *J. Comp. Physics.* 23 (1977) 263.
10. Van Leer B., *J. Comp. Physics.* 23 (1977) 276.
11. Van Leer B., *J. Comp. Physics.* 32 (1979) 101.
12. Roe P. L., *J. Comp. Physics.* 43 (1981) 357.
13. Collela P., Glaz H., *J. Comp. Physics.* 59 (1985) 264.
14. Glaister P., *J. Comp. Physics.* 74 (1988) 382.
15. Liou M., Leer B. V., Shuen J., *J. Comp. Physics.* 87 (1990) 01.
16. Gallouet T., Masella J. M., *C. R. Acad. Sci. Paris.* 01 (1996) 77.
17. Carter J. E., *NASA TR R-385* (1972).
18. Rizzetta D. P., Visbal M. R., Gaitonde D. V., *J. AIAA.* 39 (2001) 2283.
19. Tenaud C., Garnier E., Sagaut P., *Int. J. Numer. Meth. In Fluids.* 33 (2000) 249.
20. Mallinson S. G., Gai S. L., Mudford N. R., *J. Fluid. Mech.* 342 (1997) 1.
21. Fang J., Yao Y., Zheltovodov A., Li Z., Lu L., *J. Phys. Fluid.* 27 (2015) 125101. <http://doi.org/10.1063/1.4935700>.
22. Jammalamadaka A., Li Z., Jaber F., *J. Phys. Fluid.* 26 (2014) 063601. <http://doi.org/10.1063/1.4880135>
23. Yang G., Yao Y., Fang J., Gan T., Li Q., Lu, L., *Chinese Journal of Aeronautics (CJA).* 29 (2016) 617. <http://dx.doi.org/10.1016/j.cja.2016.04.001>.
24. Hirsch C., *Vol. 1.* (1988).
25. Pironneau O., *J. Numer. Math.* 38 (1982) 309.
26. Hung C. M., Mc Cormack R. W., *J. AIAA.* 14 (1976) 475.
27. Steger J. L., Warming R. F., *J. Comp. Physics,* 40 (1981) 263.
28. WU M., Martin M. P., *J. AIAA.* 45 (2007) 879.
29. Babinsky H., Harvey J. K., *Cambridge University Press.* 978-0-521-84852-7 (2011).
30. Zapryagaev V. I., Kavun I. N., Lipatov I. I., *Progress In Flight Physics.* 5 (2013) 349.

(2017) ; <http://www.jmaterenvirosnci.com>